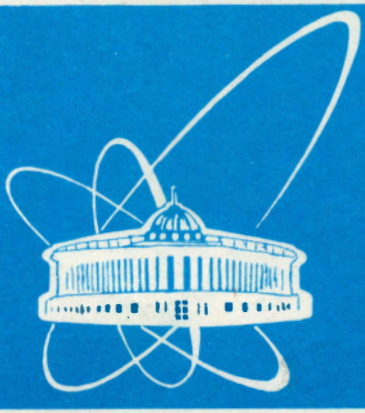

ОБЪЕДИНЕННЫЙ
ИНСТИТУТ
ЯДЕРНЫХ
ИССЛЕДОВАНИЙ

Дубна

98-294

E7-98-294

WIDE APERTURE KINEMATIC SEPARATOR **COMBAS** REALIZED ON THE STRONG FOCUSING PRINCIPLE*

Submitted to «Nuclear Instruments and Methods A»

*This work is supported in part by grant INTAS-93-496 and by grant RFBR-96-02-17214

1998

A.G.Artukh[1], G.F.Gridnev, M.Grushezki[2], F.Koscielniak[2],
A.G.Semchenkov[3], O.V.Semchenkova[3], Yu.M.Sereda[3], V.A.Shchepunov,
J.Szmider[2], Yu.G.Teterev, P.G.Bondarenko, L.A.Rubinskaya,
Yu.P.Severgin[4], Yu.A.Myasnikov[4], B.V.Rozhdestvenski[4],
A.Yu.Konstantinov[4], V.V.Koreniuk[4], I.Sandrev[5], S.Genchev[5],
I.N.Vishnevski[6]

[1]E-mail: artukh@cv.jinr.ru
[2]On leave from the Henryk Niewodniczanski Institute of Nuclear Physics, Crakow, Poland
[3]On leave from the Institute for Nuclear Research, Kiev, Ukraine
[4]Efremov Scientific Research Institute of Electrophysical Apparatus, St.Petersburg, Russia
[5]Laboratory for Technical Development of the Bulgarian Academy of Sciences, Sofia, Bulgaria
[6]Institute for Nuclear Research, Kiev, Ukraine

I. Introduction

The availability of heavy ions in the intermediate energy range offers a unique opportunity for detailed explorations of this important transition region between low energy "binary" nuclear collisions and high energy multifragmentation processes. In the transition region (20 to 100 AMeV) the projectile velocities are comparable to the characteristic velocities in nuclear matter such as the velocity of sound and the Fermi velocity of nucleons inside the nuclei. Overcoming those different thresholds may result in manifestation of qualitatively new mechanisms. The possible influence of the neutron excess $(N/Z)_p$ of projectiles and of the $(N/Z)_t$ of targets on the production cross section of unstable nuclei also remains unknown.

In the last ten years experiments have shown [1-4] that the large production cross section of projectile-like fragments at intermediate energies can be used to produce exotic nuclei with a high production rate and to form intense secondary radioactive beams. This permitted one to study the details of the boundaries of particle stability in the range of the lightest elements ($Z<5$) and to discover a number of new phenomena such as the neutron halo, multinucleon correlations, the violation of the order of filling subshells etc. It is expected that systematic investigations of the near-threshold anomalies in drip-line nuclei for heavier elements ($Z>5$) with larger "magic numbers" ($N=20,28$ etc.) can not only provide quantitative information, but also enrich our knowledge by discovering new phenomena in nuclei with the higher asymmetry of filling single-particle levels by neutrons and protons.

At the same time the large production cross section of exotic nuclei and their forward focussing promoted the development of special magnetic channels which can reject intense primary beams reliably and to separate fragments effectively by the masses [5-7].

In this report the parameters and present status of the wide aperture kinematic separator COMBAS [8], designed for experiments with intermediate energy projectiles of the U-400M cyclotron (FLNR JINR, Dubna), are presented. The COMBAS separator is planned to be used both in the mode of a high-resolving spectrometer for studying reaction mechanisms and in the mode of a prompt (in-flight) separator in experiments on the synthesis and study of the properties of short-lived exotic nuclei near the drip-lines.

2. Magnetic separation of the products of heavy ion reactions

2.1. Basic ion-optics

While discussing the first-order ion-optics of a beam in a magnetic field we use the following coordinate frame, with the horizontal plane being the plane of the fragment separation

$$X(s) = (x, \theta, y, \phi, \ell, \delta)^T,$$

where x and y are the radial and vertical displacements of the ions off the optical axis, ℓ is the path length difference between the ion trajectory and the central trajectory s, θ and ϕ are the radial and vertical inclinations of the trajectory with respect to the optical axis, and $\delta = \Delta p / p_0$ is the fractional momentum deviation of an ion from the central axis.

The equations for the beam dynamics are ordinary difference equations of the first order. So the transformation of the phase space coordinates may be written in the matrix form

$$X(s) = R(s) \cdot X(0),$$

where *X(0)* is the vector of the initial values for the phase-space coordinates, *X(s)* is the vector for point *s*.

We imply no first-order coupling between the horizontal and vertical motions, so some of the matrix elements are identical to zero:

$$R = \begin{pmatrix} R_{11} & R_{12} & 0 & 0 & 0 & R_{16} \\ R_{21} & R_{22} & 0 & 0 & 0 & R_{26} \\ 0 & 0 & R_{33} & R_{34} & 0 & 0 \\ 0 & 0 & R_{43} & R_{44} & 0 & 0 \\ R_{51} & R_{52} & 0 & 0 & 1 & R_{56} \\ 0 & 0 & 0 & 0 & 0 & 1 \end{pmatrix}$$

R_{12} and R_{34} are the sine-like particular solutions for the horizontal and vertical motions, R_{16} and R_{26} give the linear and angular horizontal dispersion for the off-momentum particles. R_{51} and R_{52} give the path length difference for the cosine-like and sine-like trajectories with respect to the central trajectory.

2.2. Resolving Power

The momentum resolving power of the separator at the dispersive focal plane F_d is given by the linear dispersion at F_d divided by the horizontal beam width:

$$R_p = \frac{R_{16}(F_d)}{\Delta x_{image}}.$$

The focal plane position is given by the zero value of the sine-like horizontal trajectory,

$$R_{12}(F_d) = 0$$

which is the beam point-to-point image, so the equation for the resolving power can be written in the following form in terms of the initial beam size and the magnification factor:

$$R_p = \frac{R_{16}}{R_{11} \Delta x_{object}}.$$

Next, to understand how to get the maximum resolving power, we use the invariant of motion, which for the point-to-point image looks like

$$R_{16} / R_{11} = R_{52}.$$

Finally we have the following equation for the resolving power, with the path length difference for the sine-like trajectory as the quotient.

$$R_p = \frac{R_{52}(F_d)}{\Delta x_{object}}.$$

The resolving power is usually calculated for the beam width equal to 1 mm, which makes it possible to compare different separators.

This value can be calculated using the following equation as an integral along the central trajectory of the ratio of the sine-like trajectory and the bending radius of the dipole magnets:

$$R_{52}(F_d) = \int_0^{F_d} R_{12}(s) / \rho(s) ds.$$

It is obvious from the equation that the sine-like trajectory inside the bending magnets should be increased in order to increase the resolving power. That is the main conclusion with respect to the resolving power.

The sine-like trajectory can be increased in various ways. The most common one is to have quadrupole lenses installed ahead of the bending magnets.

2.3. Momentum Acceptance

The moment offset of a fragment leads to the radial displacement of the trajectory off the optical axis by the following value

$$\Delta x(s) = R_{16}(s)\delta.$$

So, an increase in the momentum spread of the accepted beam results in the radial aperture of the magnets being increased, which substantially increases their weight.

There is another problem. The large value of the momentum spread gives rise to the nonlinear beam distortions, so-called chromatic aberrations.

How to cope with these problems, which limit the momentum acceptance of the separator? The only cure is the use of low-dispersive optics for the device. This can preserve the rather moderate value of the dispersion function and maximize the resolving power by minimizing the magnification factor.

2.4. Solid Angle Acceptance

The beam sizes within the separator can approximately be calculated in terms of the sine-like trajectories using the following equations

$$\tilde{x}(s) \cong R_{12}(s)\theta$$
$$\tilde{y}(s) \cong R_{34}(s)\phi$$

It should be pointed out that the horizontal sine-like trajectory should be rather large to produce the large value of the momentum resolving power. So, increasing the solid angle acceptance of the machine, we increase the beam sizes. This results in the larger weight of the magnets, which grows like θ^2, and the larger power consumption of the magnets, which grows like ϕ^2.

Those two factors are technical limitations. There is a third one. Large displacements off the channel axis give rise to the so-called geometrical optical aberrations of the beam, which drastically distort the beam. Sometimes these

distortions can not be corrected by imposing the sextupole and octupole magnetic field component. It strongly depends on the first-order ion-optics design.

2.5. Energy of the ions

The magnetic rigidity of ions is the only parameter, which determines their motion in a magnetic field. The magnetic rigidity $B\cdot\rho$ is linked to the particle energy through the relativistic equation

$$B\cdot\rho = K\cdot\frac{A}{Zu}\left[\frac{E}{A}\left(1+\frac{E/A}{2Mu}\right)\right]^{1/2}$$

in which B (Tesla) is the spectrometer magnetic field

$\rho(m)$ – the radius of curvature of the mean trajectory in the magnet

Zu – the detected ionic charge of the particle

E – the energy of the particle in MeV

A – the atomic number of the particle

$\frac{E}{A}$ – the energy of the particle per mass unit

$Mu = 931.5$ MeV the atomic mass unit

$K = (2Mu/c)^{1/2} = 0.1438$

There are technical limitations (saturation of iron is one of the most important) which restrict the maximum magnetic field level for room-temperature magnets by the value of about 1.9 T. Only up to this level one can get the desired field configuration by means of the pole shaping.

Fixing the field level and increasing the momentum of the ions, one gets larger and larger bending radii inside the magnets. This gives a rise in the channel length and the aperture of the magnets, which may result in some economical problems because the weight of a magnet is scaled like magnetic rigidity to the third power $[(B\cdot\rho)^3]$ and electric power consumption is scaled like magnetic rigidity to the power of 2 to 2.5 $[(B\cdot\rho)^{2\text{ to }2.5}]$.

2.6. Requirements for the Ion-Optics of the Separator

$R_{52}(F_d) \cong 4000$ (Resolving power)

$R_{12}(F_d) = 0$ (Point-to-point image)

$R_{11}(F_d) \cong \pm 0.4$ (Low dispersive optics)

$R_{26}(F_d) = 0$ (Achromaticity)

Vertical beam waist at F_d

3. COMBAS separator design

LISE [5] had been the only achromatic fragment separator in operation at the time the COMBAS design was started [8,9]. The ion-optics design of LISE was based on the traditional scheme using two bending magnets with uniform field distribution and quadrupole lenses for producing the desired resolving power and analyzing the beam. The A1200 fragment separator [6] and the RIPS fragment-separator [7] in general are similar to LISE. The enlargement of the parameters of the latest fragment separators [6,7] makes it necessary to use sextupole lenses to correct the nonlinear distortions of the beam.

Our studies have shown that the further substantial enlargement of solid angle and momentum acceptances is not possible with the use of the traditional ion-optics design, because it leads to the great enlargement of the magnet apertures and gradients in quadrupole lenses, unachievable in room-temperature magnets, and nonlinear beam distortions become the main problem of the ion-optics.

The design goals of COMBAS made it necessary to reconsider the ion-optic schemes used for fragment separators. The only solution seemed to be realistic was the use of low-dispersive optical schemes implementing magnets with combined functions of the bending and strong focussing of the beam.

In the study of the nonlinear distortions and correction of the beam a method based on aberration theory [10,11] is used. In this method the canonical transformation of the particle phase space variables is expressed as a six-fold Tylor expansion using their initial boundary values:

$$x_i(1) = \sum_{q=1}^{\infty} \sum_{k_1 \ldots k_6 \geq 0}^{k_1+\ldots+k_6=q} \left(x_i \mid x_1^{k_1} \ldots x_6^{k_6}\right) x_1^{k_1}(0) \ldots x_6^{k_6}(0).$$

The 6-dimensional vector $X = (x_1 \ldots x_6)^T \equiv (x, p_x, y, p_y, \ell, \delta)^T$ is the vector describing the location of a particle in phase space.

In the linear approximation:

$$\left.\begin{array}{l} x \cong \text{radial} \\ y \cong \text{vertical} \\ \ell \cong \text{longitudinal} \end{array}\right\} \text{displacements}$$

$$\left.\begin{array}{l} p_x \cong \theta \\ p_y \cong \phi \\ \delta \cong \Delta p / p \end{array}\right\} \text{canonical momenta.}$$

3.1. COMBAS design goals

Resolving power

$$R_p \cong 4000$$

Momentum acceptance

$$\frac{\Delta p}{p} = \pm 10\%$$

Solid angle acceptance of about 6.4 msr

$$\theta = \pm 40 \text{ mrad}$$
$$\phi = \pm 40 \text{ mrad}$$

Maximum magnetic rigidity of ions

$$(B\rho)_{max} = 4.5 \text{ Tm}$$

3.2. Magneto-optical structure of the COMBAS separator

The magnetic structure of the COMBAS in-flight separator with triple focussing in the final position (F_a) is formed by a cascade of eight magnets with nonuniform magnetic fields. Functionally, the $M_1M_2M_3M_4F_dM_5M_6M_7M_8F_a$ magneto-optical configuration (Fig.1a) is composed of two analogous sections (with four magnets M_1-M_4 and M_5-M_8 in each sections) placed symmetrically with respect to middle plane F_d (dispersive focal plane). The first section M_1-M_4, playing the role of a magnetic rigidity filter, provides the collection of the radioactive nuclei and the spatial separation of the nuclei from the incident beam (rejection). The second section M_5-M_8 compensates the dispersion due to the first section and analyzes nuclei at the achromatic focus F_a (Fig.1b).

For the first time the ion-optics of the separator has been designed using the strong focussing principle, which was realized on the base of four 25° multipole analyzing

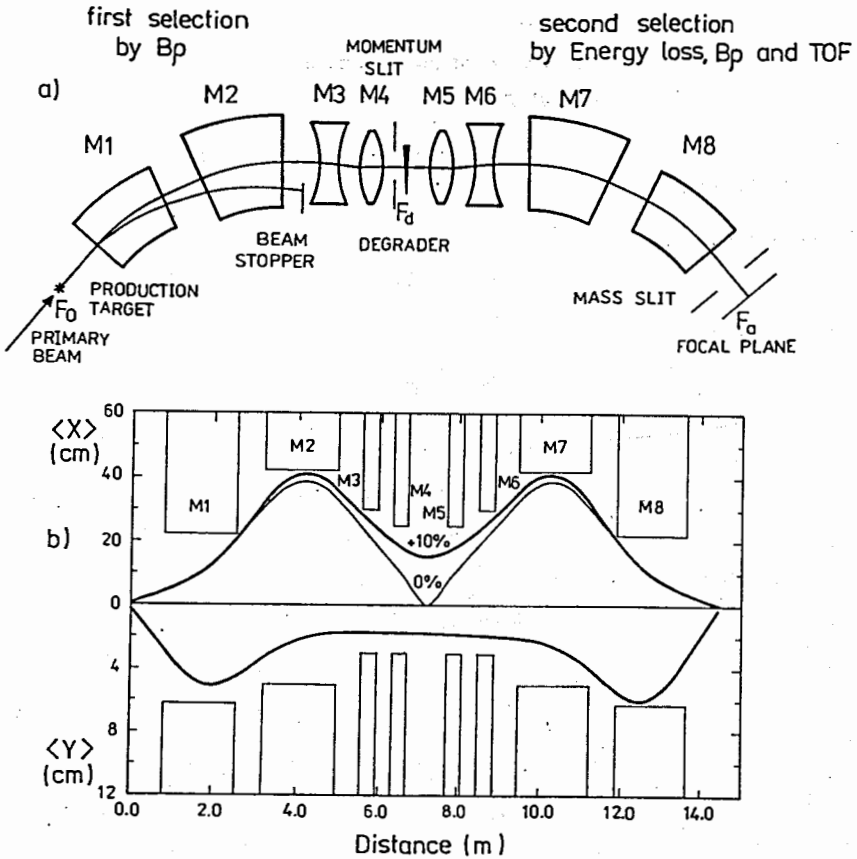

Fig. 1. a) Magneto-optical sketch of the fragment-separator COMBAS;
b) The horizontal X and vertical Y beam envelopes of the magnetic channel. The solid thick line is the contour of the $\delta = \pm 10\%$ momentum acceptance; the thin line corresponds to $\delta = 0\%$.

magnets (M_1M_2 and M_7M_8) with nonuniform magnetic fields and of four 7.5° dipole correcting magnets (M_3M_4 steering pair and M_5M_6 steering pair) [12,13].

3.3. Transfer Matrices

$$R(F_d) = \begin{pmatrix} -0.36 & 0 & 0 & 0 & 0 & 153 \\ -0.014 & -2.78 & 0 & 0 & 0 & 0 \\ 0 & 0 & -6.05 & 39 & 0 & 0 \\ 0 & 0 & -0.014 & -0.08 & 0 & 0 \\ -2.3 & -436 & 0 & 0 & 1 & -56 \\ 0 & 0 & 0 & 0 & 0 & 1 \end{pmatrix}$$

$$R(F_a) = \begin{pmatrix} 1 & 0 & 0 & 0 & 0 & 0 \\ 0.01 & 1 & 0 & 0 & 0 & 0 \\ 0 & 0 & -0.06 & -6.1 & 0 & 0 \\ 0 & 0 & 0.164 & -0.06 & 0 & 0 \\ 0 & 0 & 0 & 0 & 1 & -119 \\ 0 & 0 & 0 & 0 & 0 & 1 \end{pmatrix}$$

x, y, and ℓ in [cm]

θ and ϕ in [rad]

3.4. Correction of the aberration effects

The ion-optics analysis shows that nonlinear effects substantially reduce the resolving power of separators using wide-aperture magnets. The main contribution to the beam distortions is made by the (x/xp_x), (x/p^2_x), $(x/p_x\delta)$ second-order aberrations and the (x/p_x^3), $(x/p^2_x\delta)$ and $(x/p_x\delta^2)$ third-order aberrations. In order to improve focussing properties of the bending magnets and to achieve the optimal minimization of the aberration effects, we divided the analyzing magnets in each section into two magnets M_1M_2 (the first section) and M_7M_8 (the second section).

The compensation of the second-order and third order aberrations was fulfilled by three iterations. The required values for the correcting sextupole and octupole components of the magnetic field are provided by the special profiling of the pole pieces of the $M_1M_2(M_7M_8)$ magnets (the main first iteration). The correcting sectupole and octupole components of the magnetic field for the $M_3M_4(M_5M_6)$ magnets are introduced by two methods by the special profiling of the pole pieces and by providing the necessary curvature for the entrance and exit pole boundaries, which

effects the beam of particles as a thin sextupole and octupole lens. The final formation of the required magnetic field distribution is achieved by the fine tuning of the magnetic field with additional small correcting coils installed on the pole faces of the M_4M_5 magnets (the third iteration). The latter iteration also allows one to minimize the effects of the degrader, the non-accuracy of the manufacturing of the pole profiles and the non-accuracy of the assembling of the magnetic channel.

Careful numerical two (2D)- and three (3D)-dimensional simulations were carried out to provide the required magnetic field distributions and to analyze the fringe field in the end regions of the magnets [14]. The latter is especially important for the $M_3M_4(M_5M_6)$ magnets because of their small length. The ferromagnetic saturation effects were taken into account. When studying nonlinear beam distortions, we assumed that the particles were uniformly distributed in the volume, which was defined by the following inequalities

$$\left.\begin{array}{l} x^2+y^2 \le r^2,\ r=0.25\,\text{cm} \\ p_x^2+p_y^2 \le p^2,\ p=0.04\,\text{rad} \end{array}\right\} \text{Uniform.}$$

The distribution by δ was also assumed to be uniform within the limits

$$\delta \in [-0.06,+0.06]$$

By the three-coordinate manufacturing of the pole pieces, the high order aberrations were minimized in the M_1-$M_4(M_5$-$M_8)$ wide-aperture magnets. The complicated multipole structure of the $M_1M_2(M_7M_8)$ magnets operating with the sign alternating magnitude of gradients demanded carrying out highly precise three-component magnetic measurements (the future publication) to reproduce the real magnetic field distribution needed for the trajectory analysis of particles. The final processing of the entrance and exit boundaries for the $M_1M_2(M_7M_8)$ magnets is to be carried out according to the results of the magnetic measurements. The results of the compensation in F_d plane of the most valuable second-order and third-order aberrations are shown in Table 1.

Table 1.

Most valuable second-order aberrations

	Before correction	After correction
$(x\|xp_x)$	-30.6	4.0
$(x\|p_x^2)$	-3236.0	-6.0
$(x\|p_x\delta)$	377.0	1.24

Most valuable third-order aberrations

	Before Correction	After correction
$(x\|p_x^3)$	-11701.0	2557.0
$(x\|p_x^2\delta)$	-19107.0	-4649.0
$(x\|p_x\delta^2)$	-6811.0	-1988.0

4. Present status of the COMBAS separator

4.1. Ion-optical parameters of the COMBAS separator and the parameters of the realized magnets

In Fig.2 the real magnetic configuration of the COMBAS fragment-separator is shown, which is installed on one of the extracted channel beams of the U-400M cyclotron of FLNR JINR.

The main ion-optics parameters of the COMBAS separator are listed in Table 2 and the parameters of the magnets are given in Table 3; the coefficients characterizing the magnetic fields are shown in Table 4; the power consumption of the magnets is given in Table 5.

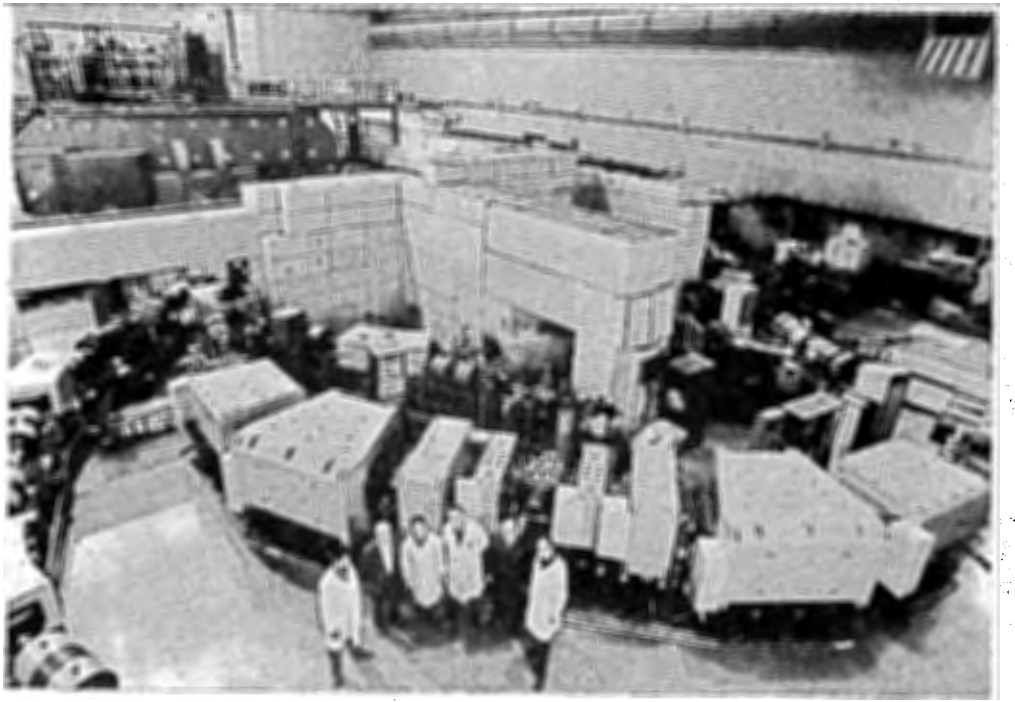

Fig. 2. View of the fragment-separator COMBAS at the experimental area of the cyclotron U-400M (beam direction from the left to the right).

Table 2
The main ion-optics parameters of the COMBAS fragment-separator

$B\rho_{max}$	[T · m]	4.5
Solid angle (maximum)	[msr]	6.4
Momentum acceptance (maximum)	[%]	20
Horizontal magnification in F_d		- 0.36
Vertical magnification in F_d		- 6.0
Momentum dispersion (in the linear approximation)	[cm/1%][a)]	1.53
Momentum resulition	[FWHM][b)]	4360
Horizontal magnification in F_a		1
Vertical magnification in F_a		1
Full length of the channel	[from F_o to F_a]	14.5

[a)] If the second-order and the third-order aberrations are taken in consideration then dispersive function for 20% momentum acceptance is described by the following square equation: $X = 1.53 \cdot \delta - 0.03 \cdot \delta^2$, where $\delta = \Delta p / p_0$

[b)] Main object slit width = 1 mm. Second-order and third-order aberrations are taken into account.

Table 3
Parameters of the COMBAS magnets

Parameter	M_1; M_8	M_2; M_7	M_3; M_6	M_4; M_5
Induction on the central trajectory, $B\rho_{max}$ [T]	1.125	1.125	1.5	1.5
Induction on the central trajectory, $B\rho_{nomin}$ [T]	0.875	0.875	1.167	1.167
Radius of the central trajectory, ρ [m]	4	4	3	3
Height of the gap along the central trajectory, h [cm]	12	10	6	6
Width of the effective working area [cm]	40	80	60	50
Deflection of the central trajectory	25°	25°	7.5°	7.5°

Table 4
Magnetic field characteristics of the COMBAS magnets

Magnet type	Coefficients of magnetic fields		
	n_1	n_2 [cm^{-3}]	n_3 [cm^{-4}]
$M_1(M_8)$	11.0024	0	1.67×10^{-8}
$M_2(M_7)$	-6.752	-2.77×10^{-7}	-4.02×10^{-10}
$M_3(M_6)$	0	6.69×10^{-7}	-2.38×10^{-8}
$M_4(M_5)$	0	-2.62×10^{-6}	-1.46×10^{-8}

N.B. The magnetic field in the median plane of the magnets is determined as follows: $B = B_0(1 - n_1X/R + n_2RX^2 + n_3RX^3 +...)$, where X – the radial deviation from the centre of the magnet; R – the radius of the curvature of the central trajectory; B_0 – the magnetic fields on the central trajectory; n_1, n_2 and n_3 are the field indices corresponding to the quadrupole, sextupole and octupole field components.

Table 5
Power requirement for magnets M_1-M_8

Magnet	Nominal (kWatt) ($B\rho_N = 3.5$ T · m)	Maximum (kWatt) ($B\rho_m = 4.5$ T · m)
$M_1(M_8)$	32.0	63.0
$M_2(M_7)$	30.0	60.0
$M_3(M_6)$	11.0	22.0
$M_4(M_5)$	7.0	15.0
Total M_1-M_8	160.0	320.0

The M_1-M_8 magnets are supplied by highly stabilized power supplies (better $4\cdot10^{-5}$). The vacuum pumping of the volume of the COMBAS separator is provided by eight turbopumps and is better $3\cdot10^{-6}$ torr.

The careful minimization of the main high-order aberrations permitted one to correct the orientation of the F_d dispersive focal line in such way that it is perpendicular to the ion-optics axis (to the central trajectory). This is important for positioning coordinate detectors in the F_d focal plane which measure the energy and angular distributions of fragments. In the COMBAS separator the F_d focal line is expanded up to 40 cm length to achieve 25% total momentum acceptance.

Presented in Fig.3 is the calculated collection efficiency of fragments for the indicated magnitude of the angular and momentum acceptances versus the projectile-like fragment mass produced in a fragmentation process at intermediate energy. Also shown in the same Fig.3 is the collection efficiency of nuclei for the main existing fragment-separators. The collection efficiency for different separators was calculated using experimental data on the energy and angular distributions produced in the interaction of 44 MeV/u ^{40}Ar projectiles with a ^{27}Al target [15].

The commissioning of all the apparatus complex [16] and the final testing of the parameters of the COMBAS separator using ^{14}N and ^{12}C projectiles with 40-50 AMeV energies were completed at the end of 1997. The experiments showed a good agreement of the experimental results with the project calculations as well as that the collection efficiency of the COMBAS separator for short-lived nuclei near the drip lines which are produced with wide momentum and large angular distributions is 5 and 10 times higher than those of RIPS (RIKEN, Japan) and LISE (GANIL, France) accordingly (Fig.3). The main parameters of existing and COMBAS separator are listed in Table 6 for comparison.

Table 6
Comparison of Fragment Separators

Device	$\Delta\Omega$ [msr]	$\Delta p/p$ [%]	Max. [T-m]	Res. Power
LISE	1.0	5.0	3.2	800
FRS	0.7-2.5	2.0	9-18	240-1500
A 1200	0.8-4.3	3.0	5.4	700-1500
RIPS	5.0	6.0	5.76	1500
COMBAS	6.4	20	4.5	4360

4.2. Diagnostic of incident beams and radioactive nuclear beams

Detector systems for diagnostic of incident and radioactive beams are distinguished in accordance with the difference of the beam dimensions and especially the beam intensities. Different types of profilometric detectors are used for operation modes, namely, profilometers of high intensity (up to 10^{14} pps) for incident beams and of low intensity for radioactive beams. It is desirable that, for both of the modes, diagnostic detectors should be fully transparent for fragments (non-destructive beam) and permit one to measure the time-of-flight of fragments with the aim of

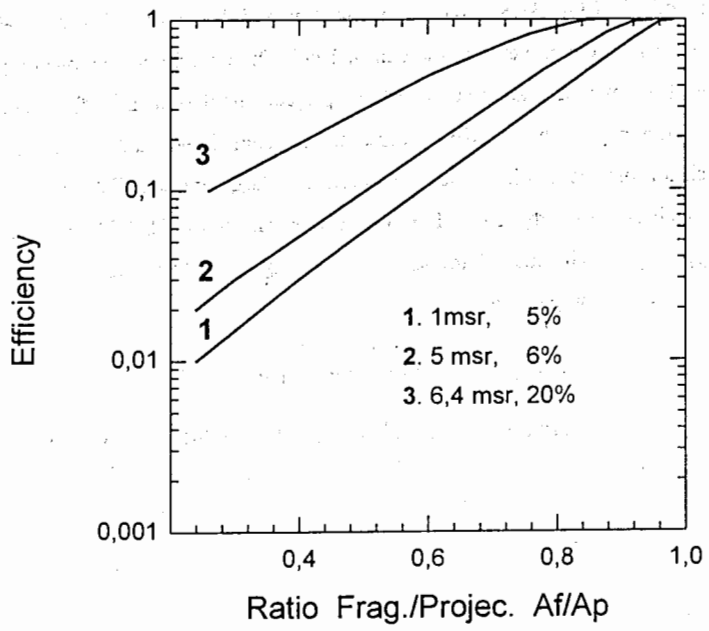

Fig.3. Calculated efficiency of the collection of the fragments produced in fragmentation processes at intermediate energies versus the projectile-like fragment mass (A_F/A_P). The efficiencies of the operating separators LISE (number 1) and RIPS (number 2) and the designed COMBAS separator (number 3).

isotopic identification (by A and Z) and also to measure the coordinates of fragments with the aim of measurement of the energy distribution of isotopes ($d^2\sigma/dEd\Omega$).

In the high intensity mode (tunning regime of the separator) we use three types of profilometers; namely, special luminophoros with videocamers, which are positioned behind each magnet including the F_d and F_a focal planes; Faraday caps and residual gas ionization detectors [17]. The first two types of profilometers operate in destructive beam mode. Those can be taken away sequencely out of the path of the incident beam. The third profilometer (non-destructive beam) is positioned ahead of and behind the target position. We also use primary beam stoppers behind the M_1 and M_2 magnets, and in the F_d place, which operate simultaneously as Faraday caps. The target is also used to measure the beam current.

In the mode of low intensity radioactive beam gas-filled counters (non-destructive beam) are used, namely, large aperture two coordinate (X,Y) avalanche counters. The (X,Y) coordinate detectors are positioned by pairs in F_d and ahead of the F_a focal planes. The pair of (X,Y) coordinate detectors operate as a track detector. In F_d two (X,Y) detectors are installed at a 170 mm distance after one another and ahead of the F_a focal plane two (X,Y) detectors are installed at 350 mm distance.

At present the positional resolution of the profilometers is equal to 2 mm (step grid) in the F_d plane and 1 mm in the F_a plane.

4.3. Degrader system

It is known that a lot of nuclei produced in fragmentation reactions have the same magnetic rigidity. Using only a magnetic field, it is impossible to separate a monoisotope. The achromatic magnetic channel (fragment-separator) can easily be reorganized so as to be operated in the regime of an isotopic separator if the energy loss degrader located in the F_d intermediate focal plane will be used [18,19]. We have used the conception of "momentum-loss achromat" in designing the COMBAS separator. The crucial point for such a type of separation is the thin profile of the degrader foil. It's thickness should be chosen so as to provide a separation of isotopes of different sort, and simultaneously the profile should be optimized to preserve the achromaticity of the magnetic channel minimizing the energy and angular straggling of ions. The achromaticity of the degrader means that the dispersion matching before and after the degrader is not disturbed. It should be pointed out that the power of

rejection of an admixture depend strongly the relations of the intensities for separated isotopes. In these cases the needed rejection can be obtained by the special adjusting of the profile and the thickness of the degrader. For the wide-aperture COMBAS separator it presents additional technical problems of manufacturing a degrader of a very large size (X=400 mm, Y=70 mm) and of fine profiling in the case of relatively thin degrader foil.

We have developed a computer code to provide degrader optimization and to study beam dissipative optics with a degrader. The beam optics before and after the degrader is treated using a matrix formalism including non-linear effects up to the third order. The passing of a beam through the degrader is simulated by the Monte Carlo algorithm including stopping power data table. The material of the degrader was chosen to be aluminium to minimize the effects of secondary reactions and to provide the required accuracy of the degrader profile in manufacturing. The initial spatial distribution of ions was supposed to be uniform within the acceptance of the separator: $x^2 + y^2 \le r^2$ (r = 0.25 cm) and $p_x^2 + p_y^2 \le p^2$ (p=0.04 rad).

The required separation of heavy isotopes ^{40}Ar, ^{41}K, ^{39}Ar, ^{37}Cl, ^{38}Ar and ^{36}Cl produced in the reaction ^{40}Ar (44 AMeV) + ^{9}Be (99 mg/cm^2) was realized for the following parameters of an Al wedge: the degrader thickness for the central trajectory is equal to 0.35 mm and the wedge angle is 0.8 mrad [18]. Experiments on the optimization of the degrader profile are now being continued in the different ranges of fragment mass using different projectiles.

4.4 Detecting system

The detecting system for the COMBAS facility consists of two types of counters fulfilling different functional purposes.

The track (x, y) coordinate avalanche counters measure the (Δx, Δy) position of a fragment in the F_d plane (or ahead of F_a), $\Delta E/\Delta x$ ionization stopping power for identification of the atomic number (Z) of fragment and a Δt short timing signal used for start – stop the TDC converter, which measures the (ΔT) time-of-flight of each fragment on the distance between F_d and F_a focal planes. The pair of the (x, y) counters determine the (Δx_1, Δy_1, $\Delta E/\Delta x_1$, Δx_2, Δy_2, $\Delta E/\Delta x_2$, $\Delta\theta_x$, $\Delta\varphi_y$) parameters of the detected fragment. The Δx position together with the Bρ magnetic rigidity determines the energy spectrum of a fragment ($d^2\sigma/dEd\Omega$) and $\Delta\theta_x$ (in F_d) determines

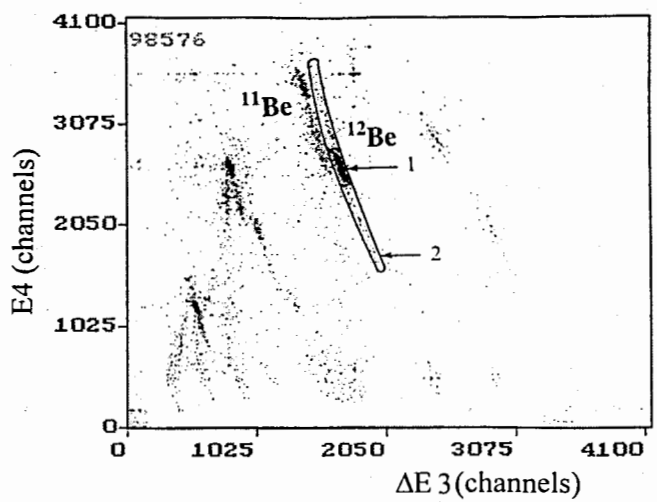

Fig. 4. The registrated two-dimensional isotopic distribution (ΔE_3 (3.5 mm), E_4 (7.5 mm)) accumulated for 2% momentum acceptance (number 1) and 20% momentum acceptance (number 2). The magnetic rigidity was tuned to the optimal yield of the ^{11,12}Be nuclei produced in the reaction ^{18}O (35·A·MeV) + ^{9}Be (1 mg/cm^2).

the angular distribution of the fragment ($d\sigma/d\Omega$). The latter is based on the use of the angular magnification in the F_d plane ($\Delta\theta_{Fd} \approx 2.8 \cdot \Delta\theta_{Fo}$). It is important because at the zero-angle COMBAS installing it permits one to measure the precise angular distributions of fragments in condition of the total rejection of the intensive primary beam. In inverse kinematic reactions (projectile heavier target) the angular acceptance of the COMBAS separator scopes the full angular distribution of fragments in the CM. The $\Delta E/\Delta x$ parameter provides hard identification of the Z atomic number of the fragment. The accuracy of the $\Delta E/\Delta x$ measurement by the avalanche counter is better than 20%. The pair of the (x, y) detectors ahead of the F_a focal plane measure the orientation of the trajectory of exotic nuclei, which is important to study the elastic and inelastic scattering of unstable nuclei or to measure the angular correlation of the charged ejectiles of decaying exotic nucleus.

The telescope of four (ΔE_1, ΔE_2, ΔE_3, E_4) silicon detectors positioned in the F_a focus is used in order to obtain correct isotopic identification of fragments by A and Z. (ΔT) time-of-flight measurement for the large momentum acceptance COMBAS separator is very important because the energy spectrum of neighboring isotopes for the total energy acceptance (40%) can get mixed. The Fig.4 illustrates the real view of the distribution of events obtained as the sum of two dimensional (ΔE_3, E_4) plots for the same magnetic rigidity which were accumulated both for 2% momentum acceptance (number 1) and 20% momentum acceptance (number 2).

5. Outlook for the experimental programme

The research programme consists of two parts:

1. Study of the reaction mechanism in the interval of intermediate energies, especially, the Fermi energy domain.
2. Investigation of the particle stability limits and a study of the properties of unstable nuclei near and beyond the drip-lines as well as mass measurements of exotic nuclei near the drip-lines.

In the investigation of the reaction mechanism of the production of exotic nuclei we want to obtain the answers to the following questions:

1. How rapidly does transition occur from the binary low energy regime to the multifragmentation high energy regime?

2. What new phenomena may occur near the sound velocity threshold and the Fermi velocity threshold?
3. How do the neutron excess $(N/Z)_p$ of projectiles and the $(N/Z)_t$ of targets influence the production cross section of exotic nuclei?
4. Why are weakly-bound nuclei produced with maximum cross sections at the energy of projectiles in the Fermi energy domain? What influence have such collective nucleon effects as nuclear sound waves and the Fermi nucleon motion?
5. How are produced extremely weakly-bounded nuclei (nearly cold) in nucleus-nucleus collisions with rather high intermediate energy?

Using ^{18}O, ^{22}Ne, $^{34,36}S$, $^{36,40}Ar$ and $^{40,48}Ca$ projectiles at intermediate energies (20÷80 AMeV) and a ^{9}Be light target and a ^{181}Ta heavy target, we plan to carry out:

1. Near zero-angle measurements of energy, angular, isotopic and element distributions for both a projectile-like and target-like fragments;
2. Study of the cross-section evolution depending on the projectile energies;
3. Study of the influence of the neutron excess of projectiles and targets.

The available experimental information is enough to study the details of the evolution of the reaction mechanism from the low energy "binary" regime to the high energy multifragmentation regime. The experimental information to be obtained is important for choosing the optimal projectile-target combination needed for the synthesis of unknown the drip-line nuclei predicted by theories.

Then the research programme is to be concentrated on the direct synthesis of unknown unstable nuclei along the drip-lines in the region of light elements with $Z<20$ as well as on the study of the properties of exotic nuclei near the closed shells N=20, 28 for elements of the O-Cl group.

Experimentalists have observed the effect of large prolate deformation in the ^{31}Na – ^{32}Mg region, where one would normally expect to find a spherical shape for the ground state due to the completion of the N=20 closed shell. The fact that N=20 is no longer "magic" for such neutron-rich nuclei came as a complete surprise because this deformation could not have been predicted from what had been known about the other nearby nuclei lying closer to the beta-stability line. If it is an overall trend for very weakly-bounded nuclei, then we can expect maximum discrepancy between the theory and experiment for extremely unstable nuclei on the drip-line with the "common magic" shell of N=20 and 28. The effect of the enhancement of binding

beyond magic shells is very important because the theoretical prediction of the position of the neutron drip-line may be mistaken, and then we can expect that the next heavier isotopes (beyond shells) are stable.

We plan to synthesize the heaviest isotopes of the O, F and Ne elements lying beyond the neutron drip-lines predicted by modern mass models. In these experiments, it is necessary to use the fragmentation of the ^{48}Ca projectile. Then comparison of the experimental data with the theoretical predictions for testing current mass models is to be fulfilled.

6. Future developments

The high intensity primary beams with 30-80 AMeV energy range, wide spectrum of accelerated ions (especially rare stable isotopes ^{18}O, ^{22}Ne, ^{26}Mg, ^{34,36}S and ^{48}Ca) of the U400M cyclotron in conjunction with the COMBAS high effective in-flight separator offer unique possibilities for producing and forming high intensity radioactive nuclear beams. This permits one to study the boundary of the particle stability in the light element range (with $Z \leq 30$) and to start the systematic study of the structure of exotic nuclei and nuclear states with extreme N/Z value.

As a new focal plane detector [20], we continue designing a multilayer drift chamber (in the regime of time-projection chamber TPC). As a multitrack detector, the three-coordinate drift chamber is to allow one to perform not only a three-dimensional reconstruction of multiparticle processes with high space resolution but also to simultaneously realize multifold identification of the atomic number of all the fragments by dE/dx in each layer of the sensitive volume. Moreover, the considerable sizes of the gas-filled volume, where the visualization of all the tracks of multiparticle decays takes place, allow one to realize 4π-geometry registration both of an unstable nucleus and the products of its decay and, simultaneously, of the recoil protons (for example) which can appear in the case of the elastic and inelastic scattering of an unstable nucleus [21] on the hydrogen component of a target (when the chamber is filled with methane or propane). The TPC detector can operate in a magnetic field of up to 1.5 T with $\vec{B} \parallel \vec{E}$. This property is very important because it permits one to precisely measure the momentums of all the charged particles of multitrack events.

We also plan to combine the COMBAS high effective in-flight separator (as a source of exotic nuclei) "on-line" with a high precision mass-spectrometer (Penning trap tandem) to measure the masses of exotic nuclei, which is of fundamental significance. At present a great quantity of unstable nuclei near the drip-lines have been identified but their ground state masses are unknown. Modern Penning traps [22] can determine the mass of a single ion with a high accuracy [$M/\Delta M(FWHM) \geq 10^7$], which permits one to separate the mass of the isomeric and ground states of exotic nuclei.

Acknowledgements

The authors are indebted to Yu.Ts.Oganessian, N.I.Tarantin, M.G.Nagaenko and S.E.Sytchevsky for the fruitful discussions and support of this project. We would like to thank the FLNR group operating the COMBAS separator for their constant help.

References

[1] D.Guerreau, in: Proc. Int. Conference on Heavy ion nuclear collisions in the Fermi energy domain (Caen, France, May 1986) p.C4-207.

[2] D.D.Warner, in: Proc. Second Int. Conference on Radioactive nuclear beams (Louvain-la-Neuve, Belgium, August 1991) p.139.

[3] A.C.Mueller, in: Proc. Third Int. Conf. on Radioactive nuclear beams (East Lansing, USA, May 1993) p.1.

[4] H.Geissel, G.Münzenberg and K.Riisager, Ann. Rev. Nucl. Part. Sci. 45 (1995) 163.

[5] R.Anne, D.Bazin, A.C.Mueller, J.C.Jacmart and M.Langevin, Nucl. Instr. and Meth. A257 (1987) 215.

[6] B.M.Sherrill, D.J.Morrissey, J.A.Nolen, Jr.N.Orr and J.A.Winger, Nucl. Instr. and Meth. B56/57 (1991) 1106.

[7] T.Kubo, M.Ishihara, N.Inabe, H.Kumagai, I.Tanihata, K.Yoshida, T.Nakamura, H.Okuno, S.Shimoura and K.Asahi, Nucl. Instr. and Meth. B70 (1992) 309.

[8] A.G.Artukh, Yu.L.Obukhov, V.A.Shchepunov, M.G.Nagaenko, Yu.P.Severgin, V.A.Titov, V.S.Belavenko and I.N.Vishnevski, Nucl. Instr. and Meth. A306 (1991) 123.

[9] M.G.Nagaenko, Yu.P.Severgin, V.A.Titov and A.G.Artukh, Proc. 2nd European part. accelerat. Conference (EPAC-2, 90) Nice, June 12, 1990, v.2, p.1312.

[10] K.Brown, F.Rothacker, D.C.Carey and Ch.Iselin, CERN 80-04 (1980).

[11] M.G.Nagaenko and Yu.P.Severgin, Preprint NIIEFA B-0379, Leningrad (1978).

[12] V.S.Kashikhin, E.A.Lamzin, Yu.A.Myasnikov, M.G.Nagaenko, S.P.Potekhin, Yu.A.Rozhdestvenski, Yu.P.Severgin, S.E.Sytchevsky and A.G.Artukh, Proc. IEEE Trans. on Magnetics, January 1992, v.28, p.564-567

[13] S.M.Ananiev, V.S.Kashikhin, E.A.Lamzin, Yu.A.Myasnikov, M.G.Nagaenko, S.P.Potekhin, B.V.Rozhdestvenski, Yu.P.Severgin, S.E.Sytchesvky, N.F.Shilkin and A.G.Artukh, Proc.3rd European Part. Accelerat. Conference (EPAC-3, 92), Berlin, Germany, March 24, 1992, v.2, p.1370-1372.

[14] N.I.Doinikov, E.A.Lamzin, A.S.Simakov and S.A.Sytchevski, Preprint NIIEFA B-0741, Moscow, CNIIAI (1986) 13c.

[15] R.Dayras et al., Nuclear Physics A460 (1986) 299-323.

[16] A.G.Artukh et al., Reports in JINR-FLNR Scientific Report, Dubna, 1997, p.250, 252, 254, 256, 258, 260, 252.

[17] V.G.Mikhailov, L.I.Yudin, V.V.Leonov, A.A.Roshchin, V.A.Rezvov, V.I.Sklyarenko, A.N.Artemiev and T.Ya.Rakhimbabaev, Proc. of the 13th Int. Conf. "Cyclotrons and their Appl.", Vancouver, Canada, 1992, p.473

[18] M.Nagaenko, I.I.Pavletsov, Yu.P.Severgin and A.G.Artukh, Proc. 4th European Part. Accel. Conf. (EPAC-4, 94), London, June 1994, p.2057.

[19] A.G.Artukh and N.I.Tarantin, Nucl. Instr. and Meth. B126 (1997)246

[20] A.G.Artukh et al., Proc. 2nd Int. Conf. on Rad. Nucl. Beams, Louvain-La-Neuve, Belgium, August 19, 1991, p.27.

[21] A.G.Artukh et al., Preprint JINR E7-93-74, Dubna, 1993.

[22] G.Bollen, Proc. 4th Int. Conf. on Rad. Nucl. Beams, Omiya, Japan, June 3-7, 1996, p.457.

Received by Publishing Department
on October 16, 1998.

Артюх А.Г. и др. E7-98-294

Широкоапертурный кинематический сепаратор КОМБАС,
реализованный на принципе жесткой фокусировки

В ЛЯР ОИЯИ создан высокоразрешающий кинематический сепаратор КОМБАС с большим угловым и импульсным аксептансами для эффективного сбора короткоживущих ядер, которые получаются с широкими угловыми и энергетическими распределениями в реакциях с тяжелыми ионами промежуточных энергий. Впервые в мире магнитооптическая конфигурация магнитного канала сепаратора КОМБАС реализована на принципе жесткой фокусировки. Сепарация и траекторный анализ частиц магнитным каналом проводится по трем параметрам: магнитной жесткости $B\rho$, ионизационным потерям ($\Delta E/\Delta X$) в деградере и времени пролета ΔT анализируемых частиц. Сепаратор КОМБАС может быть эффективно использован как в режиме высокоразрешающего спектрометра для изучения механизмов образования ядер, так и в режиме быстрого времяпролетного сепаратора в экспериментах по синтезу и изучению свойств короткоживущих экзотических ядер вблизи границ ядерной стабильности.

Работа выполнена в Лаборатории ядерных реакций им. Г.Н.Флерова ОИЯИ.

Препринт Объединенного института ядерных исследований. Дубна, 1998

Artukh A.G. et al. E7-98-294

Wide Aperture Kinematic Separator COMBAS Realized
on the Strong Focusing Principle

The COMBAS large solid angle and high momentum acceptance and high-resolving kinematic separator has been created at the Flerov Laboratory of Nuclear Reactions, JINR, to efficiently collect extremely short-lived nuclei near the zero angle which are produced in intermediate energy fragmentation reactions with wide momentum and wide angular distributions. For the first time the $M_1M_2M_3M_4F_dM_5M_6M_7M_8F_a$ magneto-optical configuration of the COMBAS separator has been realized on the strong focusing principle. The separation and trajectory analysis of particles by the separator are carried out by three parameters: the magnetic rigidity ($B\rho$), the energy loss difference in the degrader ($\Delta E/\Delta x$) and the time-of-flight (ΔT) of the analyzed particles. The COMBAS separator can be used efficiently both in the mode of a high-resolving spectrometer to study reaction mechanisms and in the mode of an in-flight separator in experiments on the synthesis and study of the properties of short-lived exotic nuclei near the drip-lines.

The investigation has been performed at the Flerov Laboratory of Nuclear Reactions, JINR.

Preprint of the Joint Institute for Nuclear Research. Dubna, 1998